Development of Multiple-grids, Fully Coupled Numerical Ocean Modeling-An Application of Upper Ocean Responses to Typhoons

Yu-Heng Tseng[1], Sen Jan[2], I-I Lin[1], Ya-ting Chang[3], T. Y. Tang[3]
[1]Department of Atmospheric Sciences, National Taiwan University
Institute of Oceanography, Nation
[2]Institute of Hydrological and Oceanic Sciences, National Central University
[3]Institute of Oceanography, National Taiwan University

Abstract

The ocean response to typhoon Kai-tak is simulated using a 4th-order-accurate basin-scale ocean model. The model is based on a multiple-grids, fully coupled model framework which uses 1/8° horizontal resolution for the western domain and 1/4° resolution for the eastern domain, respectively. The surface winds in the typhoon Kai-tak are obtained directly from the QuikSCAT satellite images blended with the ECMWF wind fields. An intense nonlinear mesoscale eddy is generated with Rossby number O(1) and 50-100km horizontal scale south of Taiwan. Nearly inertial oscillation is clearly observed in the model. More than 8°K sea surface temperature (SST) drop is found in both observation and simulation. We attribute this significant SST drop to the influence of slow moving typhoon, initial stratification and bathymetrically-induced upwelling in South China Sea.

Key word: typhoons, ocean response

1. Introduction

It is well-known that typhoons (called hurricanes in Atlantic Ocean) draw their energy from the warm ocean. The energy input from the ocean to typhoons and associated intensification depends largely on the upper ocean heat content (Lin et al., 2005). Pre-existing ocean mesoscale features have far more important in the heat and moisture fluxes feeding the storm than just SST as noted in previous studies. Shay et al. (2000) noted an abrupt change in the intensity of hurricane Opal (9/28-10/5, 1995) when it passed over a large Warm Core Eddy (WCE). Hurricane Katrina in August 2005 also experienced very similar intensification while passing over Loop Current and WCE regions. These examples show the role of warm oceanic features in providing a positive feedback to the overlying storm by intensifying the storms.

Typhoons also cause significant SST cooling which provides negative feedback to the overlying storm by weakening the intensity of the storm. For example, satellite images show that SST dropped more than 9°C and 11°C in response to the passage of typhoons Kai-tak (Lin et al., 2003) and Ling-ling (Shang et al., 2008), respectively.

In general, the primary mechanisms accounting for typhoon-forced sea surface cooling are mixed layer depth (vertical mixing/entrainment) and thermocline depth (upwelling driven by the wind stress curl of the typhoons), exchange of air-sea heat fluxes and the storm's intensity and translation speed (Price, 1981). Intense, slowly moving typhoons usually cause larger SST response (Price, 1981). Since evaporation due to high winds over warm water sustains the thermodynamic cycle of a tropical cyclone (TC) (Emanuel, 2003). SST cooling is though to inhibit cyclone intensification, preventing the typhoons from attaining its potential intensity. When a typhoon encounters the WCE, the SST cooling may be greatly suppressed primarily due to deep mixed-layer and thermocline depths of the WCE.

Early studies of upper-ocean response to typhoons include field observations (e.g. Shay et al., 1989; Jacob et al., 2000) and three-dimensional numerical ocean models (Price, 1981). Recent studies emphasize more on the understanding of the dynamical processes/ interactions with atmosphere, ocean heat contents and ocean currents (e.g. Wu et al., 2008; Tsai et al., 2008; Oey et al., 2007; Sheng et al., 2007). Typically, the ocean's response to typhoons can be divided into two stages; forced and relaxation stages. During the forced stage, the hurricane winds drive the mixed-layer currents, SST cooling by vertical mixing (entrainment) and air-sea heat exchanges (mainly due to loss of latent heat flux). The barotropic response consists of a geostrophic current modifying the sea surface height. The relaxation stage response following a hurricane's passage is primarily due to inertial-gravity oscillations excited by the typhoon. The mixed-layer velocity oscillates with a near-inertial period and hence so does the divergence and the associated upwelling and downwelling (Tsai et al., 2008).

However, no detailed study has been emphasized on the cause and mechanism of the significant temperature drop for certain typhoons. The oceanic responses to typhoons differ from one to the other in several respects making the study of the processes difficult. It is further complicated by preexisting oceanic features that modulate the upper ocean heat, mass and momentum balance due to horizontal advection. A model that resolves these mesoscale features must be used to study the oceanic response to typhoons. Larger cooling of SST in typhoon Kai-tak is found mainly because of strong Ekman upwelling associated with the local topography in SCS and a relatively shallow and warm

mixed layer. Similar mechanism may be used to describe the unique 11°C temperature drop after the passage of typhoon Ling-ling. The typical coastal upwelling significantly enhanced the sea surface cooling.

The main objectives of this paper are (1) to study the effect of a slowly moving typhoon (typhoon Kai-tak) in the South China Sea, (2) to quantify the physical processes controlling the upper-ocean thermal structure and surface cooling during typhoon passage and (3) to assess the model's ability to reproduce the observed behavior of the oceanic responses to a typhoon without data assimilation. This paper is organized as follows: section 2 describes the passage of the typhoon Kai-tak and relevant observation. Section 3 details the model configuration and results. The mechanism causing the significant SST drop is also investigated. Summary is given in section 4.

2. Typhoon Kai-tak and observation

Typhoon Kai-Tak was a category 2 typhoon in the Saffir-Simpson hurricane scale. It lingered at a quasi-stationary slow speed (0-1.4 m/s) on the northern SCS from 5 to 8 July, 2000 before it proceeded speedily (>6.1 m/s) northwards thereafter (Central Weather Bureau, Taiwan), see Fig. 1 for the best track. Before Kai-Tak's arrival, the SCS is characterized by warm SST predominantly above 30°C. The wind speed was between 5 to 10 m/s. During 5-8, July, Kai-tak's strong wind (20-40 m/s) dominated the wind field. Immediately after Kai-Tak's departure, on 9 July, a cold SST (21.5-24°C) pool (118-120°E, 19-20.5°N) of size comparable to Kai-Tak's 150 km Radius of Maximum Wind (RMW) co-located with the typhoon's track was observed. The minimum SST of 21.5°C was found at the center (118.9°E, 19.9°N) of the cold pool. In comparison with the pre-typhoon condition (30.7°C), the SST dropped as much as 9°C.

Remote-sensed data provided unique opportunity to investigate the surface temperature drop. Two remote-sensed datasets are used in the earlier study (Lin et al., 2003), QuikSCAT, and Tropical Rainfall Measuring Mission (TRMM) Microwave Imager (TMI), respectively. They measure ocean surface wind vector (QuikSCAT) and sea surface temperature (TMI) day and night under both clear and cloudy conditions. The cloud penetrating capability of TMI allows the entire area of entrainment (location of the bloom patch) to be sensed. Here, we also use QuikSCAT to provide the wind forcing in the simulation.

3. Model simulations

3.1 Model description

The Dual-grids, Paicific Ocean Model (DUPOM) used herein is based on the fourth-order accurate, collocated Arakawa-A grid DieCAST (Dietrich/Center for Air Sea Technology) model (Dietrich et al., 2008; Tseng et al., 2005). The control volume equations include fluxes of the conservation properties (momentum, heat and salt) across control volume. The model domain covers the entire North Pacific Ocean ranging from 30°S to 60°N and from 100°E to 80°W (Fig. 2). To reduce the computational time, a duo-grid approach is adopted based on a multiple-grid framework, which uses higher resolution to resolve eddies more realistically (Dietrich et al., 2008). A 1°/8 resolution is used west of 150°E where it is needed to resolve the detailed Kuroshio and regional circulations, while a 1°/4 resolution is used east of 150°E (Fig. 2). The grids are fully two-way-coupled each coarser time step (time steps are different for both grids) with a single coarse grid overlapping (i.e. 2×2 in fine grid cells). The meander and eddy exchanges are seamless at the interface without applying intergrid sponge layers or special treatments. Further details about the multiple-grid approach can be found in Dietrich et al. (2008). Model bathymetry is interpolated from unfiltered ETOPO2 depth data supplemented with the Taiwan's National Center for Ocean Research 1-minute depth archive in the Asian seas. The vertical resolution is linear-exponentially stretched by 26 layers, with a 6 m thick top layer. Both grids share the same vertical grid. Within each grid, longitudinal resolution is uniform and latitudinal resolution is generated such that varying latitude and longitude grid increments are equal everywhere (Mercator grid).

The surface wind forcing in the based model is obtained from the interpolated monthly Hellerman and Rosentstein winds (Hellerman and Rosenstein, 1983). The Levitus'94 climatology is used to initialize the model and to determine its surface sources of heat and fresh water (e-p) using the non-damping approach described in Dietrich et al. (2004). The northern boundary is closed and the southern boundary condition (30°S) is slowly nudging toward climatology in a sponge layer. The bottom is insulated, with non-slip conditions parameterized by a nonlinear bottom drag. Sub-grid scale vertical mixing is parameterized by eddy diffusivity (for temperature and salinity) and viscosity (for momentum) using a modified Price (1981) schemes described in Sheng et al. (2006). Background lateral viscosity (or diffusivity) is 100 m^2/s and 200 m^2/s, respectively.

3.2 Initial and boundary conditions for typhoon Kai-tak simulation

We take the model year 23, July 1st as the initial conditions for the Typhoon Kai-tak's simulation. Initial temperature and salinity are based on the South East Asia Time-series (SEAT) station (116°E, 18°N) observation before typhoon Kai-tak's passage in July, 2000. All model integrations are started on July 3, 2000.

The model is then driven by fields of 10 m wind stress extracted from six-hourly 2.5° ERA40. It is well-known that the ERA40 product does not adequately resolve the tropical cyclones. In this study, we further blend the ERA-40 winds with the QuikSCAT analyzed winds. Since ERA40 is updated every six hours while the QuikSCAT wind (twice per day) provides more realistic wind field and may not be consistent with ERA40, a special smoothing procedure is performed. We take the difference between the QuikSCAT and ERA-40 winds at each of the discrete observations and times. This

difference is merged into an "extended winds window" (EWW) grid which is larger than the localized QuikSCAT wind field. The difference is then set to zero at the boundary of EWW and a Poisson spreader is applied to spread the difference between the QUikSCAT wind and the EWW grid boundaries. In order to minimize the nudging at EWW grid boundaries, the EWW should extend laterally at least an eddy size beyond the QuikSCAT wind fields. The blended wind fields are then interpolated back to the DUPOM domain.

Following Oey et al. (2006), the wind stress is calculated from the wind fields using a bulk formula:

$C_d = 0.0012, \quad |u_a| \le 11$ m/s

$= 0.00049 + 0.000065\,|u_a|, \quad 11 < |u_a| \le 19$ m/s

$= 0.00136 + 2.34\times10^{-5}|u_a| - 2.32\times10^{-7}|u_a|^2, \quad 19 < |u_a| < 100$ m/s

where $|u_a|$ is the wind speed. The maximum wind speed is ~40 m/s from the QuikSCAT. The formula incorporates the limited drag coefficient in high wind speeds (Powell et al. 2003). All wind stresses are assumed to be in dynes/cm-cm and to have magnitude less than 100dynes/cm^2.

3.3 Model results

Fig. 3 shows the sea surface height superimposed by the surface velocity vector after 90 hour (i.e. July 6, 2000). The eye-wall winds drive a strongly-out-of balance cyclonic flow, as indicated by the vectors that reveal a big outward flow component of the cyclonic spinning water. The very intense nonlinear mesoscale vortex has scale 50-100 km.

During the passage of typhoons, sudden change of the surface wind stress could generate inertial motions in the upper ocean (Gill, 1982). In the north SCS, the averaged inertial period is about 35 hr (20°N). We further compare the model velocities with those measured at the ADCP mooring station KA1 (under Kuroshio Upstream Dynamics Experiment, KUDEX). To separate rapidly fluctuating inertial motions from otherwise relatively low frequency inertial currents, we applied a 6 hour low-pass filter to the observed currents. Fig. 4 shows the comparison between the modeled and observed currents. Both model and observation show clear inertial oscillations ~32 hr.

Two extremely surface cooling events after the passage of typhoons occurs (>9°C) in SCS (Lin et al., 2003; Sheng et al., 2008), including typhoon Kai-tak. How did such a drastic response happen? Entrainment mixing is in general the primary mechanism accounting for the SST response (Price, 1981). However, for a slow-moving cyclone (translation speed <4 m/s), such as, Kai-Tak, strong upwelling occurs with entrainment and the response is significantly enhanced (Price, 1981). The maximum cooling (and upwelling) is in a ring around the core of the typhoon which appears to start in the northeast corner of the typhoon where wind forced upslope flow may be involved (Fig. 5). This appears to have been forced by the inertial dynamics of a fast current by the winds up the shelfslope in the northeastern SCS. The return flow downslope can also create strong eddies by release of potential energy, thus giving some significant mixing.

Fig. 6 shows 90 hour vertical subsidence calculated at 45 m depth. It is clear to see strong vertical upwelling when the typhoon hovered in the northeastern SCS. The maximum vertical velocity can reach 30m/day (negative subsidence is upward) near the center of typhoon. Further, the continuous Ekman pumping is also enhanced by the topographical upwelling which can be seen in Fig. Fig. 7 further shows the bottom currents along the topography. Very strong alongshore currents are associated with strong upward motion near the Philippine coastal shelf. The isobaths are also shown in Fig. 7.

4. Summary

We illustrate an application of a multiple domains modeling development work using the simulation of the ocean response to typhoon Kai-tak. An intense nonlinear mesoscale eddy is generated with O(50-100km) horizontal scale in the northeastern SCS. Inertial oscillation is clearly observed. More than 8°K sea surface temperature (SST) drop is found in both observation and simulation. This significant SST drop results from the influence of slow moving typhoon, initial stratification and bathymetrically-induced upwelling in the region where the typhoon hovered.

5. References

Dietrich, D.E., R.L. Haney, V. Fernandez, S.A. Josey, and J. Tintore, (2004), Air-sea fluxes based on observed annual cycle surface climatology and ocean model internal dynamics: A precise, non-damping zero-phase-lag approach applied to the Mediterranean Sea, J. Mar. Syst. 52, 145-165.

Dietrich, D. E., Y.-H. Tseng, R. Medina, S. A. Piacsek, M. Liste, M. Olabarrieta, M. J. Bowman, and A. Mehra, (2008), Mediterranean Overflow Water (MOW) simulation using a coupled multiple-grid Mediterranean Sea/North Atlantic ocean model, J. Geophys. Res., 113, doi:10.1029/2006JC003914..

Emanuel, K., (2003), Tropical cyclones. Annual Rev. Earth Planet. Sci., 31, 75-104.

Hellerman, S., and M. Rosenstein (1983), Normal monthly wind stress over the world ocean with error estimates, J. Phys. Oceanogr, 13, 1093-1104.

Lin, I-I, C.-C. Wu, K. A. Emanuel, I-H. Lee, C. Wu, and F. Pan, (2005), The interaction of supertyphoon Maemi (2003) with a warm ocean eddy, Mon. Wea. Rev., 133, 2635-2649.

Lin, I-I, W.T. Liu, C.C. Wu, G.T.F. Wong,C. Hu, Z. Chen, W.D. Liang, Y. Yang, and K.K. Liu, (2003), New evidence for enhanced ocean primary production triggered by tropical cyclone, Geophys. Res. Lett., 30, 1718, doi:10.1029/2003GL017141.

Oey, L.-Y., T. Ezer, D.-P. Wang, S.-J. Fan, and X.-Q. Yin, (2006), Loop Current warming by Hurricane Wilma, Geophys. Res. Lett., 33, L08613, doi:10.1029/2006GL025873.

Oey, L.-Y., T. Ezer, D.-P. Wang, X.-Q. Yin, and S.-J.

Fan., (2007), Hurricane-induced motions and interaction with ocean currents. Cont. Shelf Res. 27:1249-1263.

Powell, M.D., P.J. Vickery, and T.A. Reinhold, (2003), "Reduced drag coefficient for high wind. speeds in tropical cyclones" Nature, 422, March 20 pp.279-283

Price, J. F., (1981), Upper ocean response to a hurricane. J. Phys. Oceanogr., 11, 153–175.

Shang, S., L. Li, F. Sun, J. Wu, C. Hu, D. Chen, X. Ning, Y. Qiu, C. Zhang, and S. Shang, (2008), Changes of temperature and bio-optical properties in the South China Sea in response to Typhoon Lingling, 2001, Geophys. Res. Lett., 35, L10602, doi:10.1029/2008GL033502.

Jinyu Sheng, Xiaoming Zhai, Richard J. Greatbatch, (2006), Numerical study of the storm-induced circulation on the Scotian shelf during hurricane Juan using a nested-grid ocean model, Prog. Oceanogr., 70, 233-254.

Sheng, J., L. Wang, S. Andréfouët, C. Hu, B. G. Hatcher, F. E. Muller-Karger, B. Kjerfve, W. D. Heyman, and B. Yang, (2007), Upper ocean response of the Mesoamerican Barrier Reef System to Hurricane Mitch and coastal freshwater inputs: A study using Sea-viewing Wide Field-of-view Sensor (SeaWiFS) ocean color data and a nested-grid ocean circulation model, J. Geophys. Res., 112, C07016, doi:10.1029/2006JC003900.

Tsai, Y. L., C.S. Chern and J. Wang, (2008), The upper ocean response to a moving typhoon, J. Oceanogr., 64, 115-130.

Tseng, Y.-H., D.E. Dietrich, J.H. Ferziger, (2005), Regional circulation of the Monterey Bay region-hydrostatic versus non-hydrostatic modeling, J. Geophy. Res., 110, C09015, doi:10.1029/2003JC002153.

Wu, C.-R., Y.-L. Chang, L.-Y. Oey, C.-W. J. Chang, and Y.-C. Hsin, (2008), Air-sea interaction between tropical cyclone Nari and Kuroshio, Geophys. Res. Lett., 35, L12605, doi:10.1029/2008GL033942.

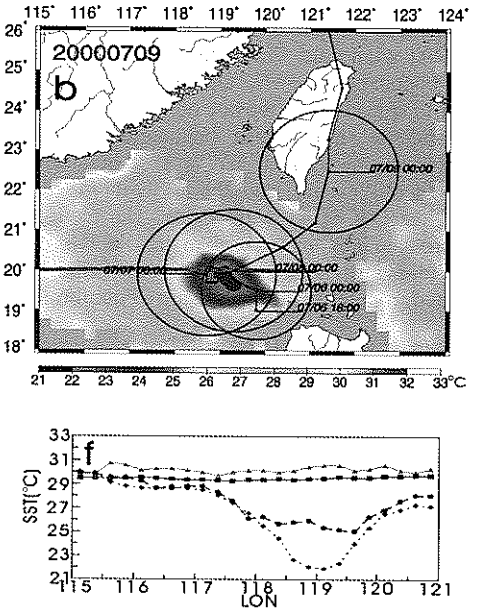

Fig. 1 (top) TRMM TMI/SST image on 9 July, 2000; (bottom) Comparisons along 20°N, pink: 7/1-7/3, 2000, Brown: 7/9, 2000, Green: 7/12-14, 2000, Blue 3-year (1998, 1999, 2001) climatological average of SST for July (Lin et al., 2003).

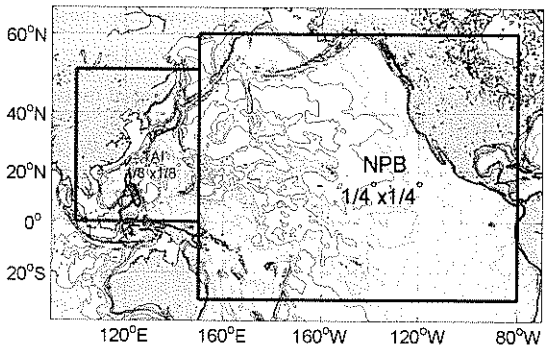

Fig. 2 Model domain and resolution.

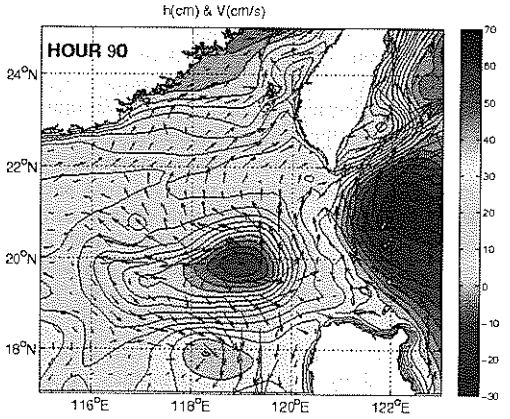

Fig. 3 Sea surface height superimposed by surface velocity vector.

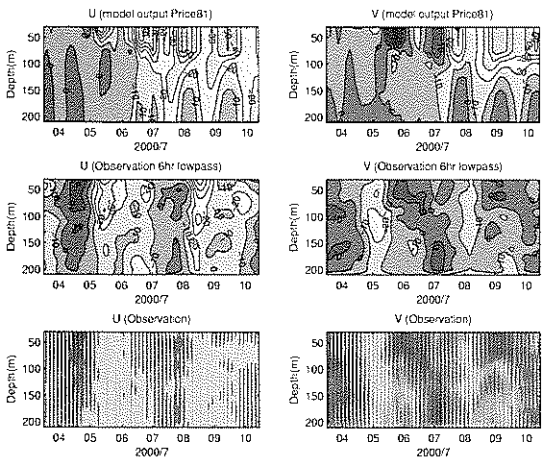

Fig. 4 Comparison between the modeled and observed velocity components.

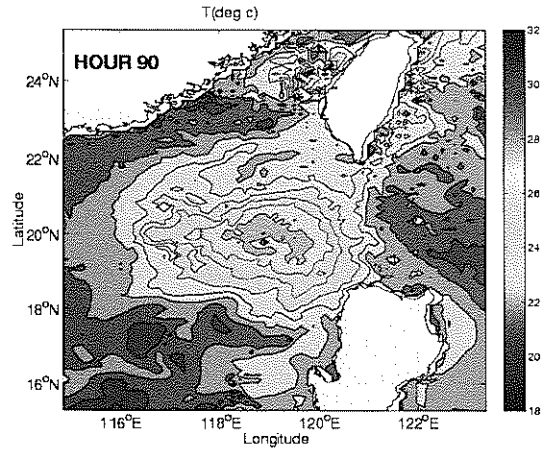

Fig. 5 Modeled sea surface temperature on hour 90.

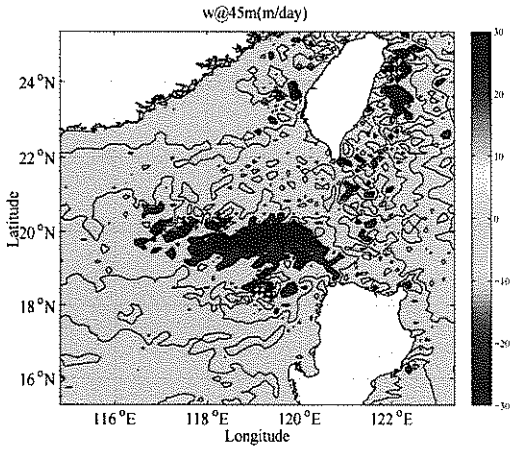

Fig. 6 Daily averaged vertical subsidence on day 4 at 45 m.

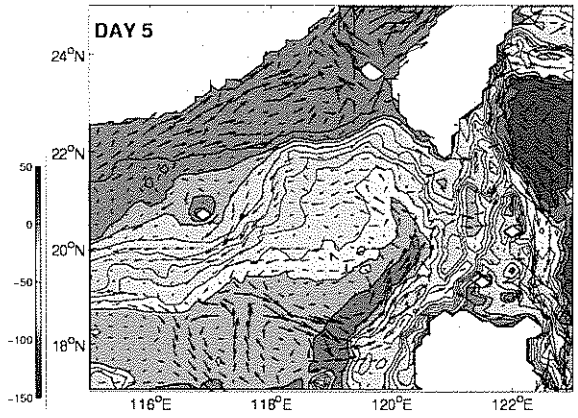

Fig. 7 bottom current vectors above the bathymetry. Isobaths are shown in color.